REVIEWS of MODERN PHYSICS

October–December 2013
Volume 85, Number 4

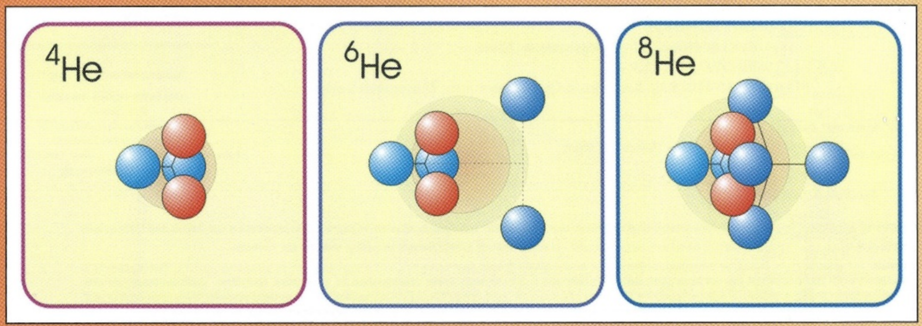

COLLOQUIUM: LASER PROBING OF NEUTRON-RICH NUCLEI IN LIGHT ATOMS

Published by American Physical Society

Argonne NATIONAL LABORATORY

... for a brighter future

U.S. Department of Energy

UChicago Argonne LLC

Office of Science
U.S. DEPARTMENT OF ENERGY

A U.S. Department of Energy laboratory managed by UChicago Argonne, LLC

Simple Atom, Extreme Nucleus: Laser Trapping and Probing of He-8

Zheng-Tian Lu

Argonne National Laboratory

University of Chicago

Funding: DOE, Office of Nuclear Physics

Quantum Monte Carlo Calculations of Light Nuclei

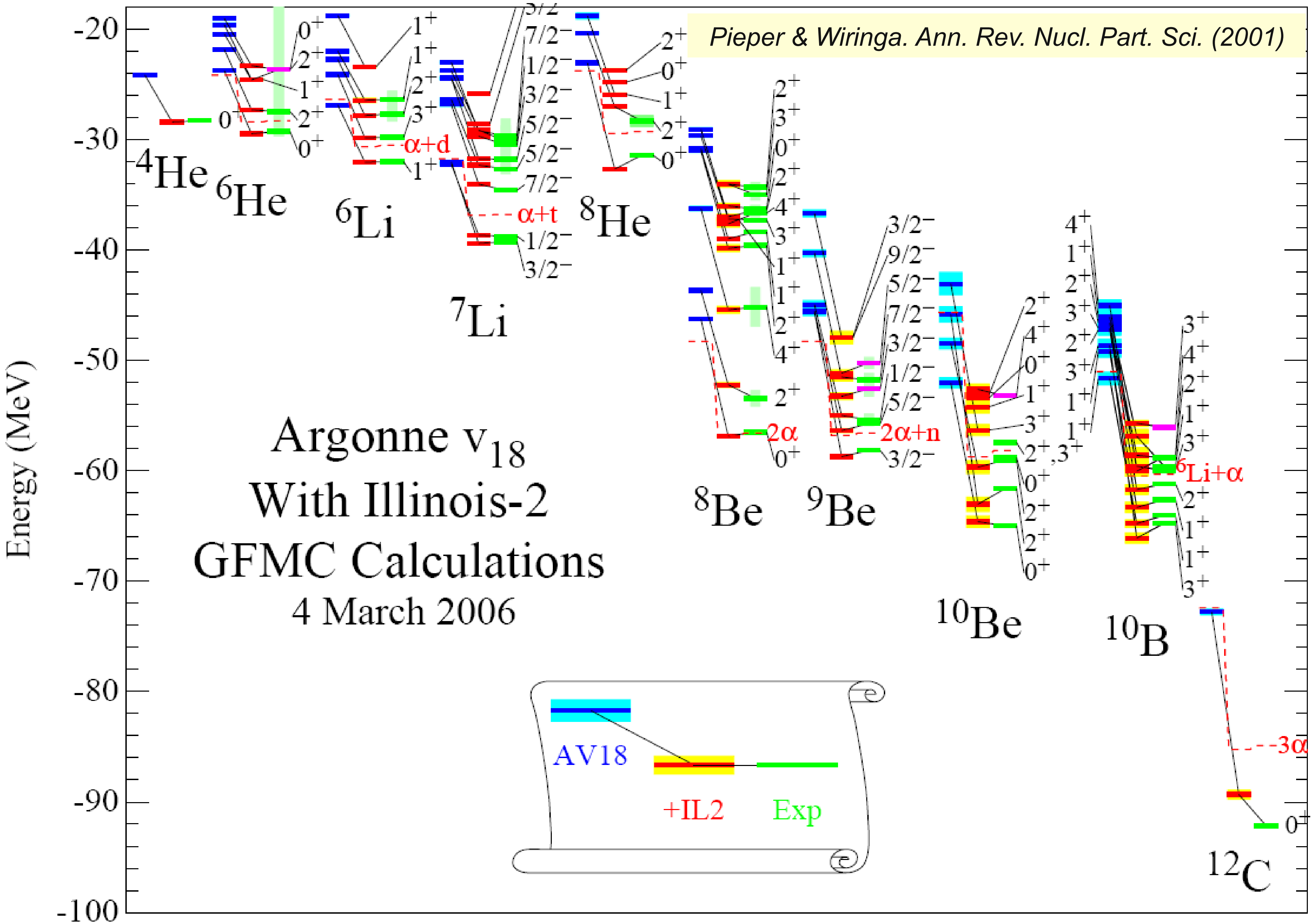

Halo Nuclei ^{6}He and ^{8}He

Isotope	Half-life	Spin	Isospin	Core + Valence
He-6	0.8 s	0^+	1	$\alpha + 2n$
He-8	0.1 s	0^+	2	$\alpha + 4n$

Quantum Monte Carlo calculation

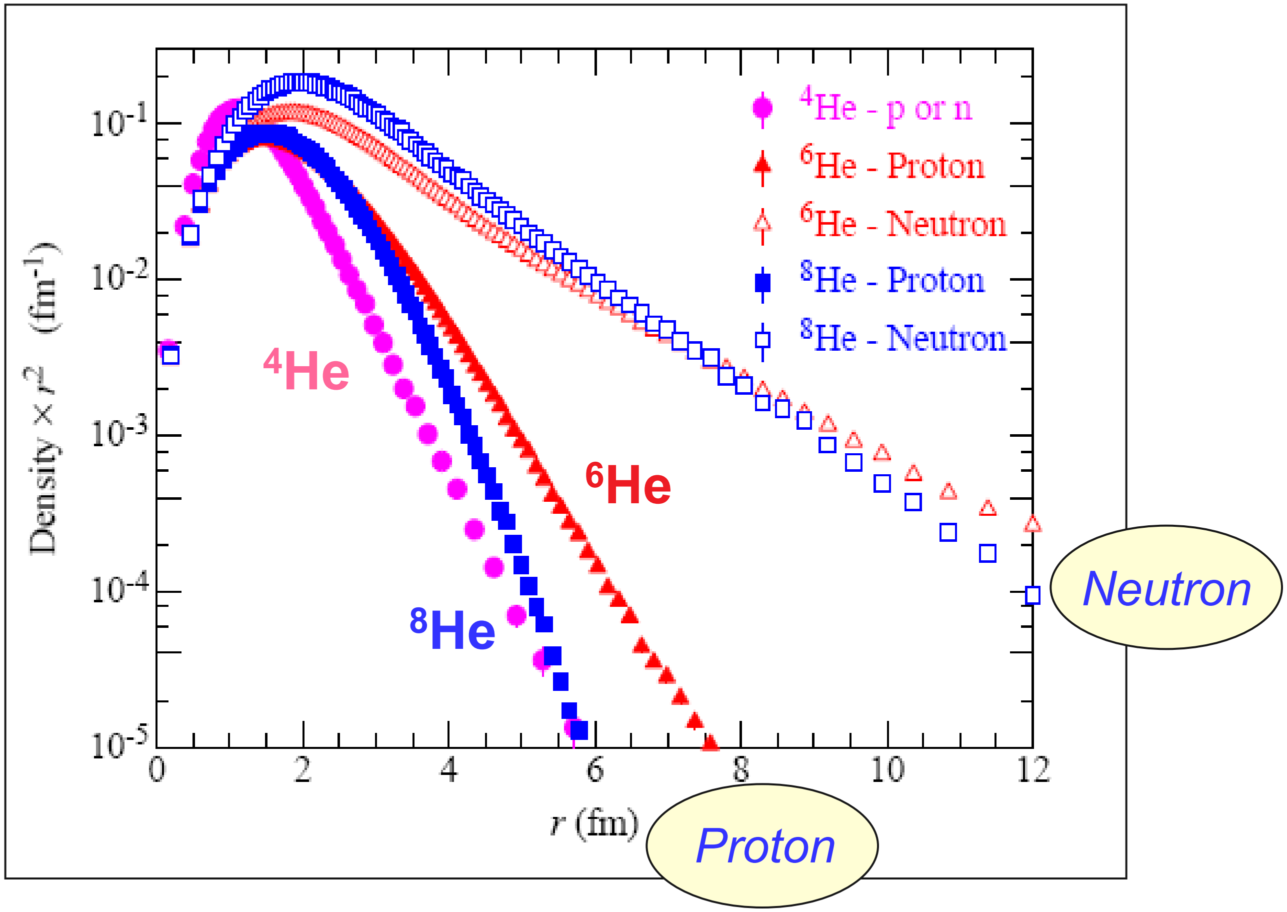

Nuclear Volume Effect

$$\delta\nu_{FS} = -\frac{2\pi}{3} Ze^2 \cdot \Delta\left|\Psi(0)\right|^2 \cdot \delta\left\langle r^2 \right\rangle$$

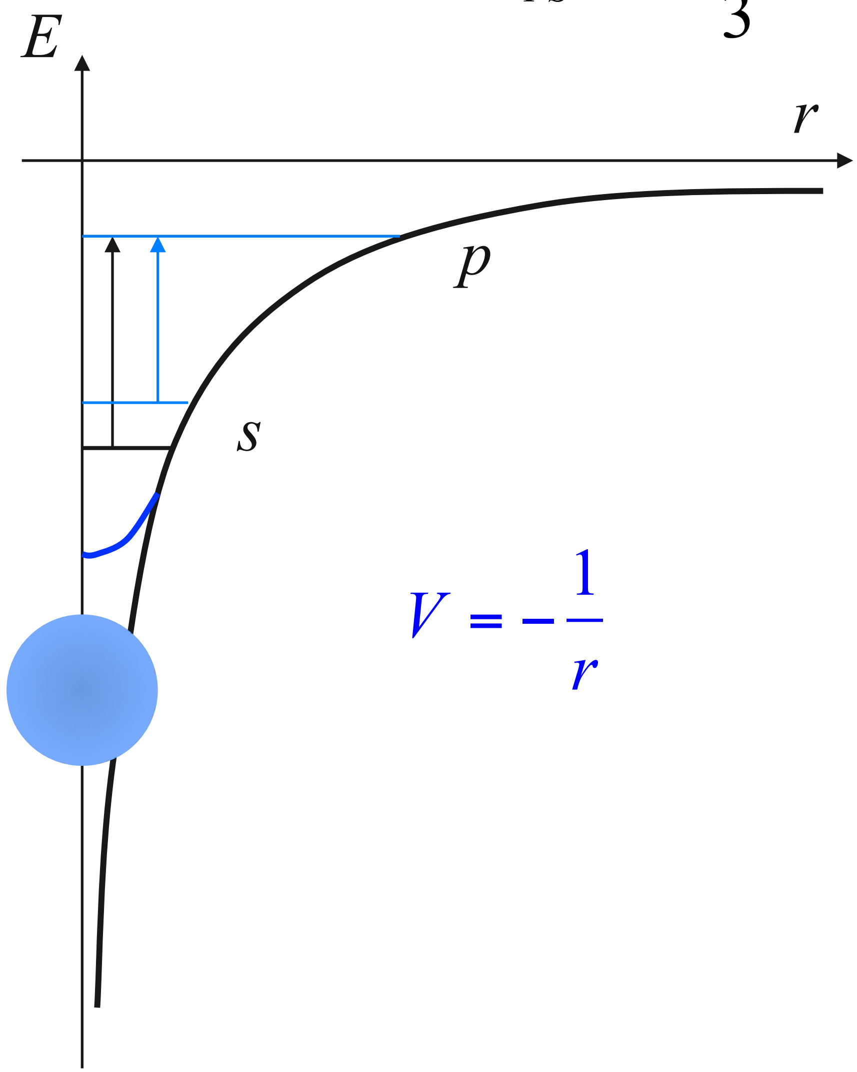

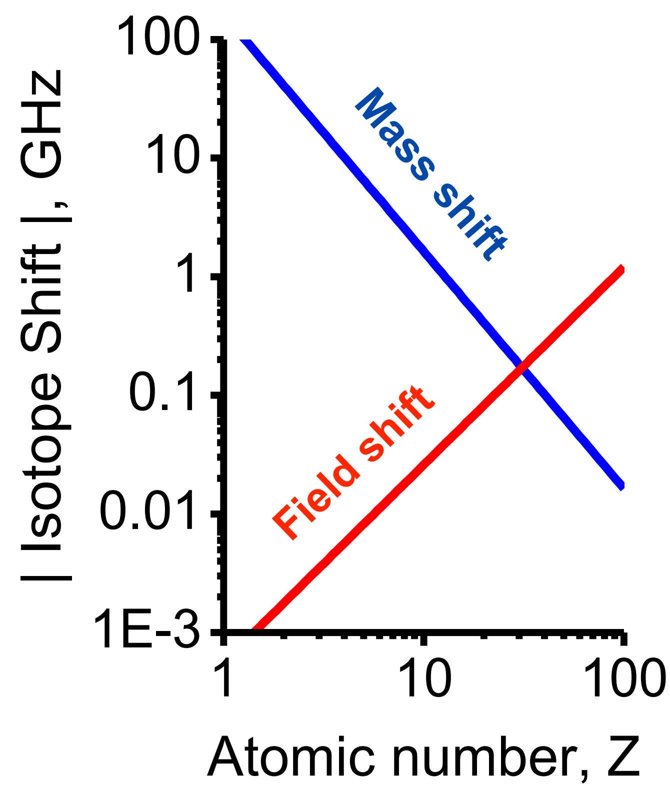

Atomic Theory of Helium

Drake, Can. J. Phys. (2006);
Pachucki & Sapirstein, J. Phys. B (2002)

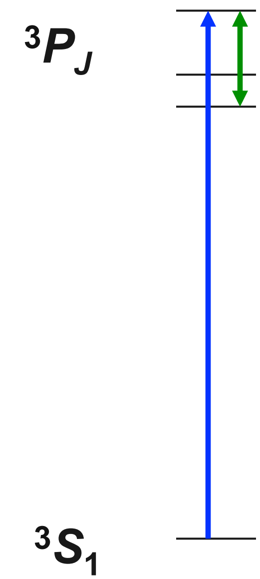

- Perturbation theory with corrections:
  - relativity
  - QED
  - *finite nuclear mass*
  - *nuclear charge radius*
- Uncertainty on transition frequency: ~ MHz
- Uncertainty on isotope shift: (MHz) x (m_e/M_N) → kHz

Isotope Shift **dn = $\mathbf{dn_{MS}}$ + $\mathbf{dn_{FS}}$**

For $2^3S_1 - 3^3P_2$ transition @ 389 nm:

^{6}He - ^{4}He : $\delta\nu_{6,4}$ = 43196.171(2) MHz – 1.010 ($<r^2>_{c,6} - <r^2>_{c,4}$) MHz/fm^2

^{8}He - ^{4}He : $\delta\nu_{8,4}$ = 64702.509(2) MHz – 1.011 ($<r^2>_{c,8} - <r^2>_{c,4}$) MHz/fm^2

100 kHz error in IS → ~ 1% error in radius

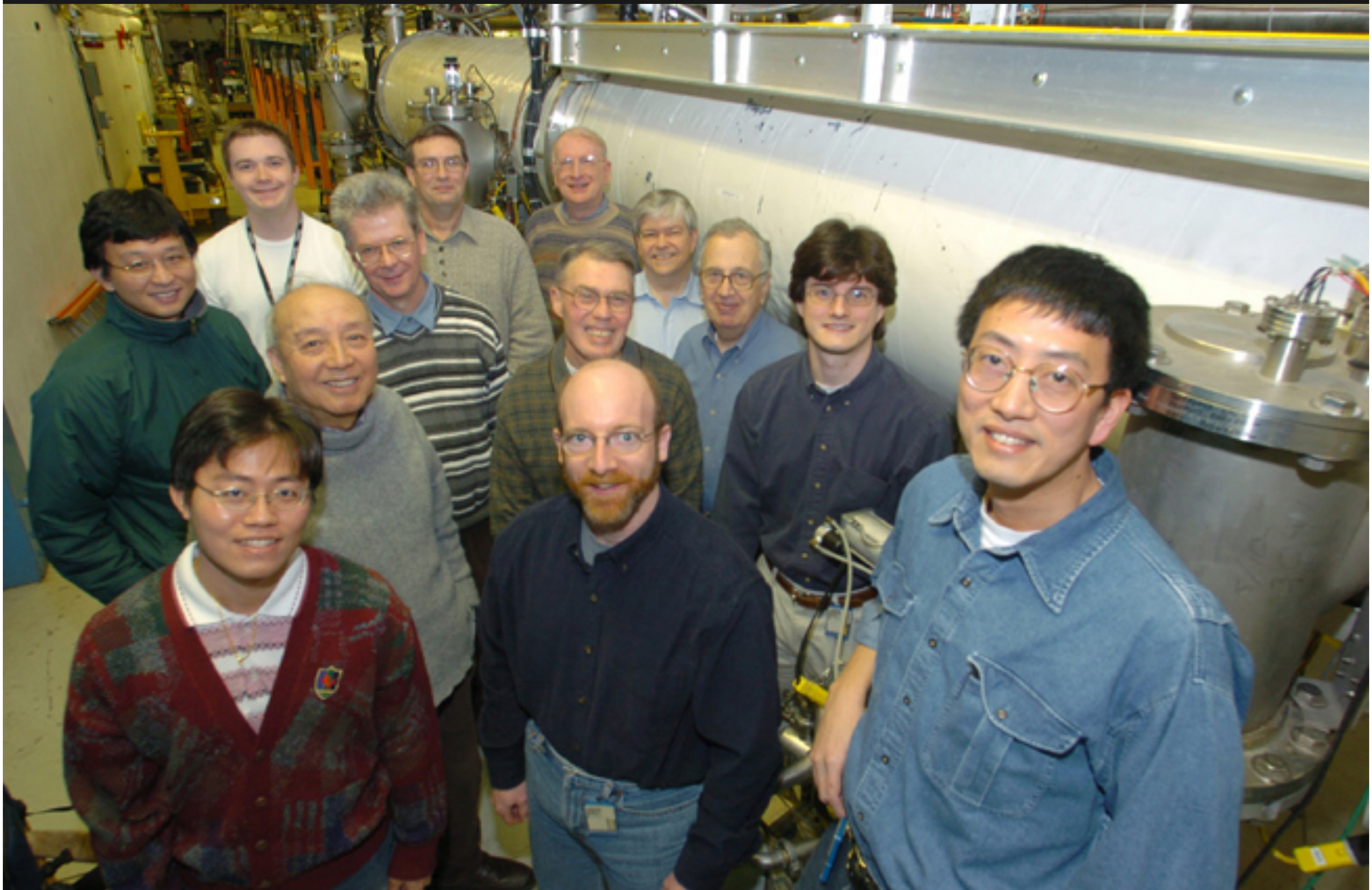

^{6}He @ ATLAS (2005)


“As a user of Ptolemy, a code developed by Steve, I appreciate his great contribution to the community.” – Xiaodong Tang

He-6 Collaboration

P. Mueller, L.-B. Wang, K. Bailey, J.P. Greene, D. Henderson, R.J. Holt, R. Janssens, C.L. Jiang, Z.-T. Lu, T.P. O'Conner, R.C. Pardo, K.E. Rehm, J.P. Schiffer, X.D. Tang - *Physics, Argonne*
G. W. F. Drake - *Univ of Windsor, Canada*

He-8 Collaboration

P. Mueller, K. Bailey, R. J. Holt, R. V. F. Janssens, Z.-T. Lu, T. P. O'Connor, I. Sulai - *Physics, Argonne;* **M.-G. Saint Laurent,** ***J.-Ch. Thomas, A.C.C. Villari*** **-** *GANIL, Caen, France*
G. W. F. Drake - *Univ of Windsor, Canada* **L.-B. Wang –** *Los Alamos Lab*


Jan. 26th 2007

Atom Trapping of ^{6}He & ^{8}He at GANIL (2007)

Atom Trap Setup

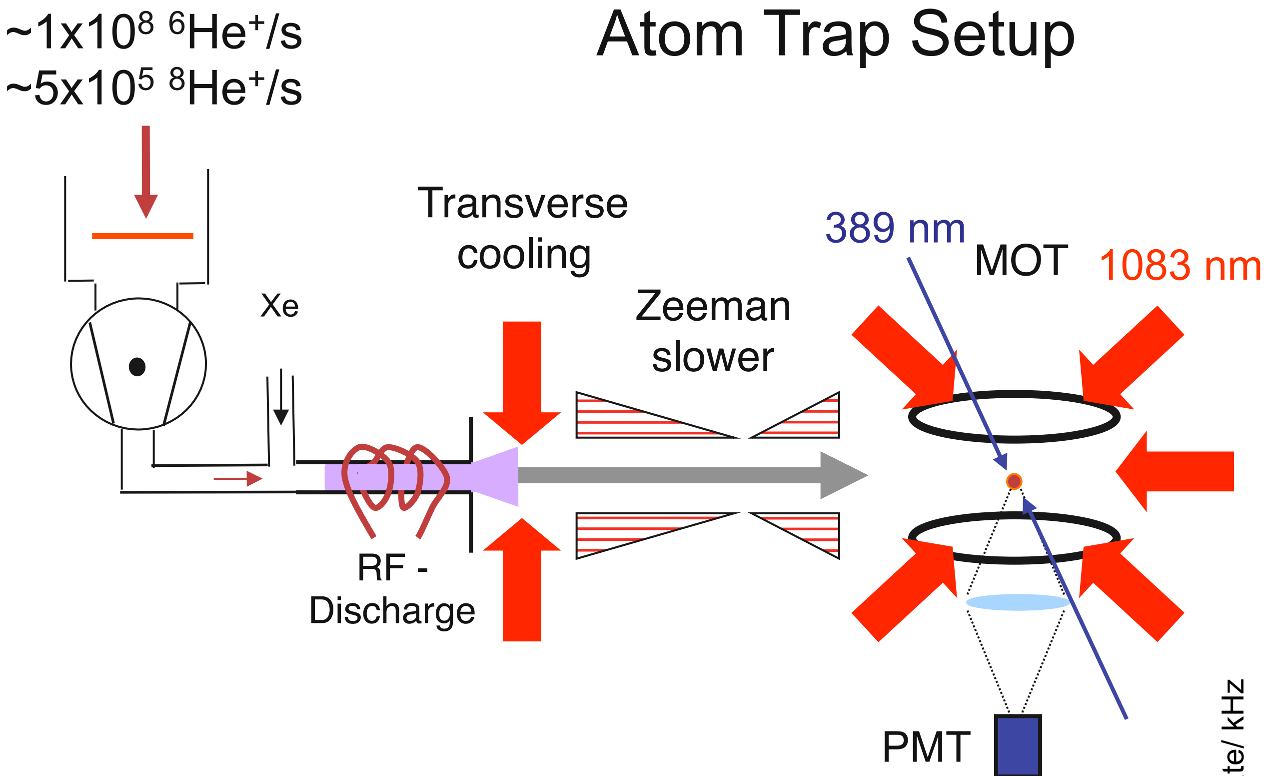

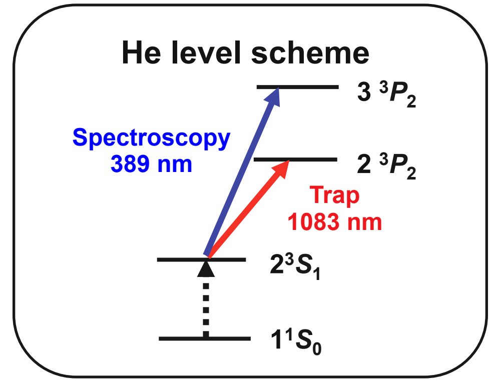

Source
^{6}He ~ 5×10^{7}/s
^{8}He ~ 1×10^{5}/s

Capture efficiency
1×10^{-7}

Trap
^{6}He ~ 5 /s
^{8}He ~ 1×10^{-2}/s

One trapped ^{6}He atom

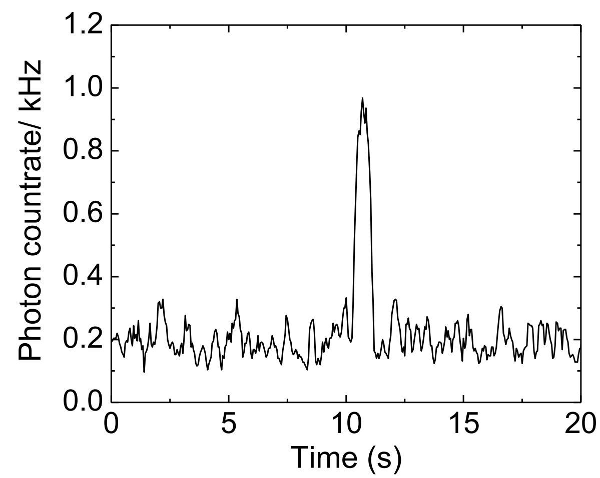

He-8 Trapped!

First He-8 Atom
June 15th 2007

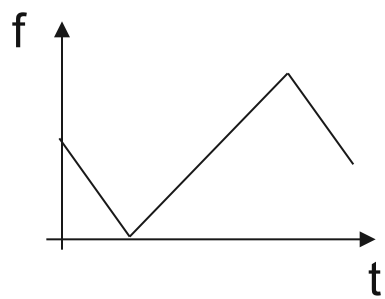

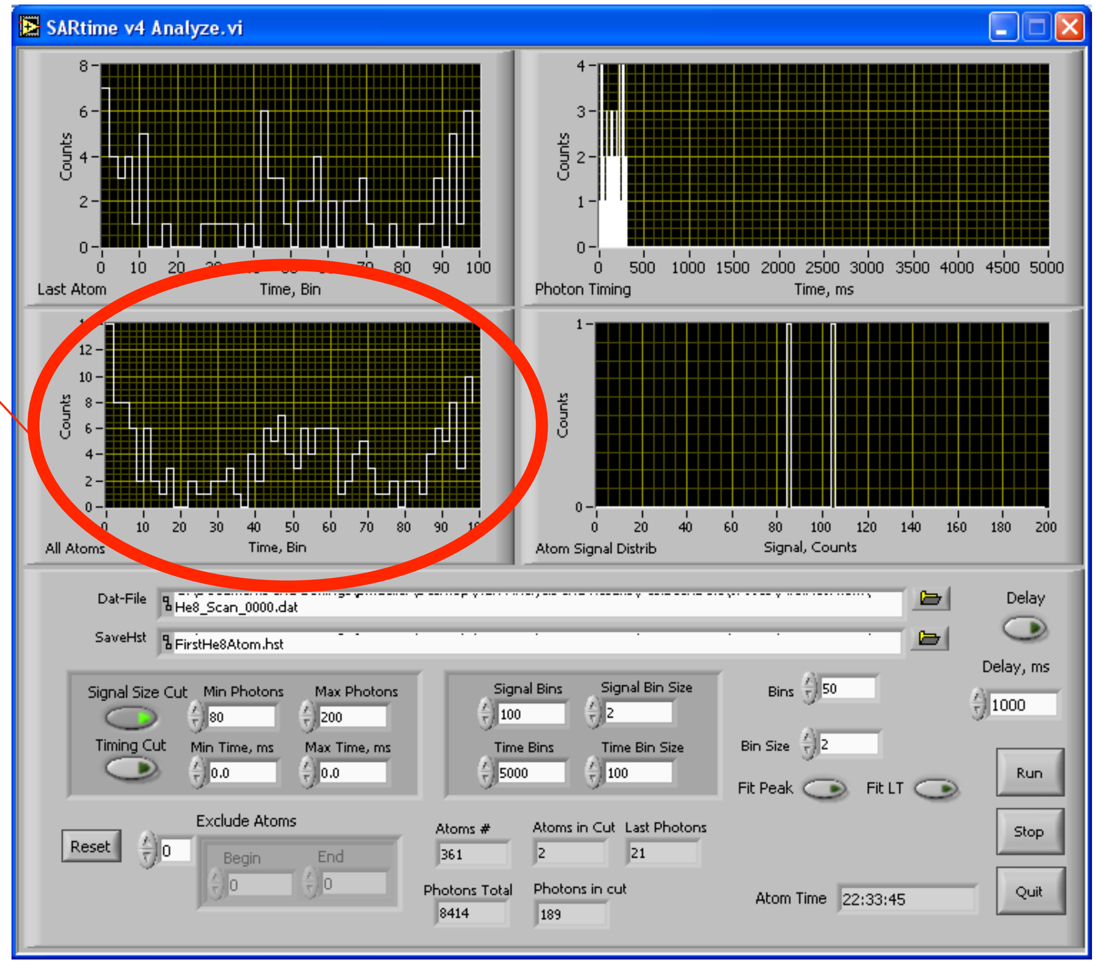

^{6}He

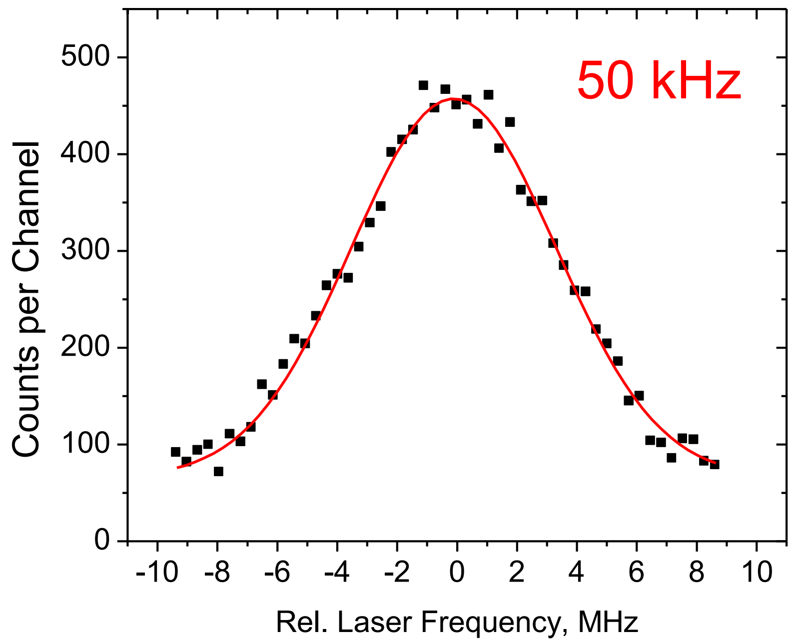

~30 ^{6}He atoms/s

^{8}He

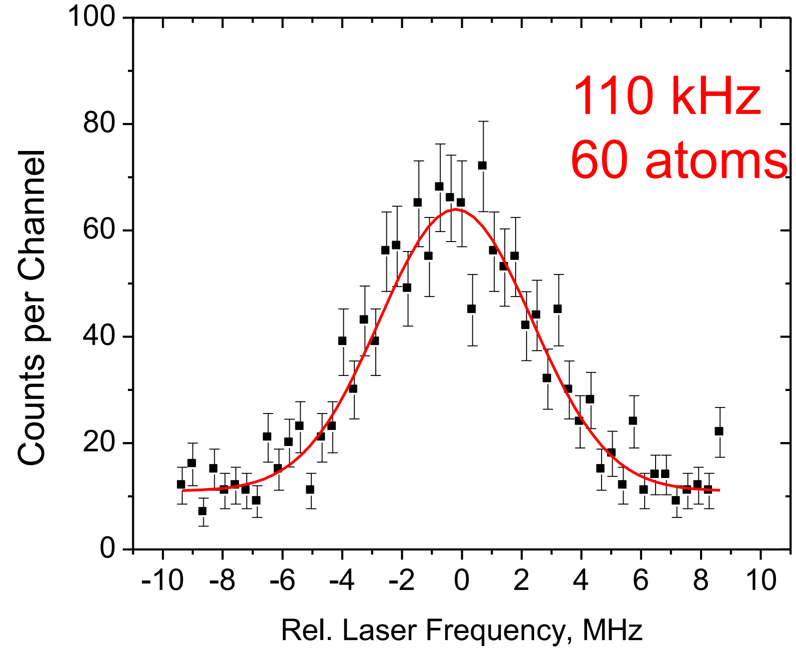

~30 ^{8}He atoms/hr

For $2^3S_1 - 3^3P_2$ transition @ 389 nm:

^{6}He - ^{4}He : $\delta\nu_{6,4}$ = 43196.171(2) MHz – 1.010 ($\langle r^2\rangle_{c,6} - \langle r^2\rangle_{c,4}$) MHz/fm^2

^{8}He - ^{4}He : $\delta\nu_{8,4}$ = 64702.509(2) MHz – 1.011 ($\langle r^2\rangle_{c,8} - \langle r^2\rangle_{c,4}$) MHz/fm^2

Field Shifts:

^{6}He - ^{4}He : $\delta\nu_{6,4}$ = 1.430 (7) [30] MHz

^{8}He - ^{4}He : $\delta\nu_{8,4}$ = 1.020 (42) [45] MHz

Proton and Matter Radii of ^{6}He & ^{8}He

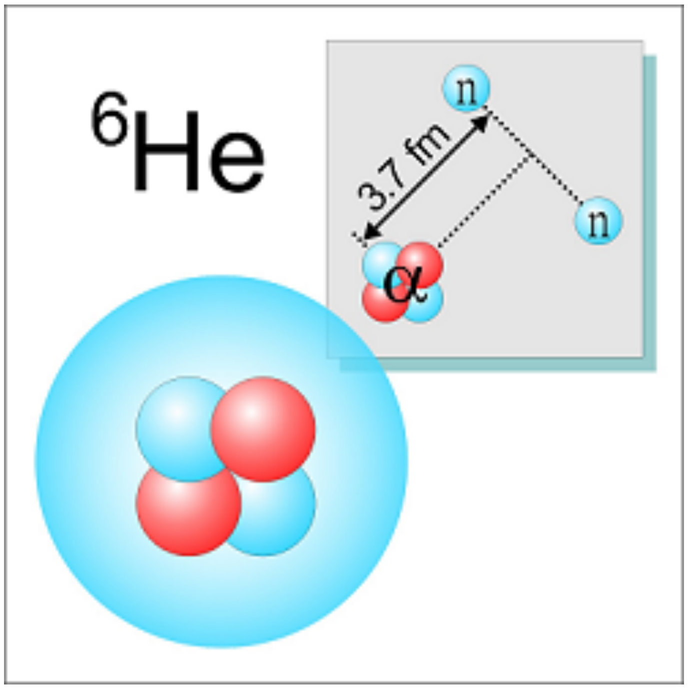

Wang *et al*., PRL (2004)
Mueller *et al*., PRL (2007)

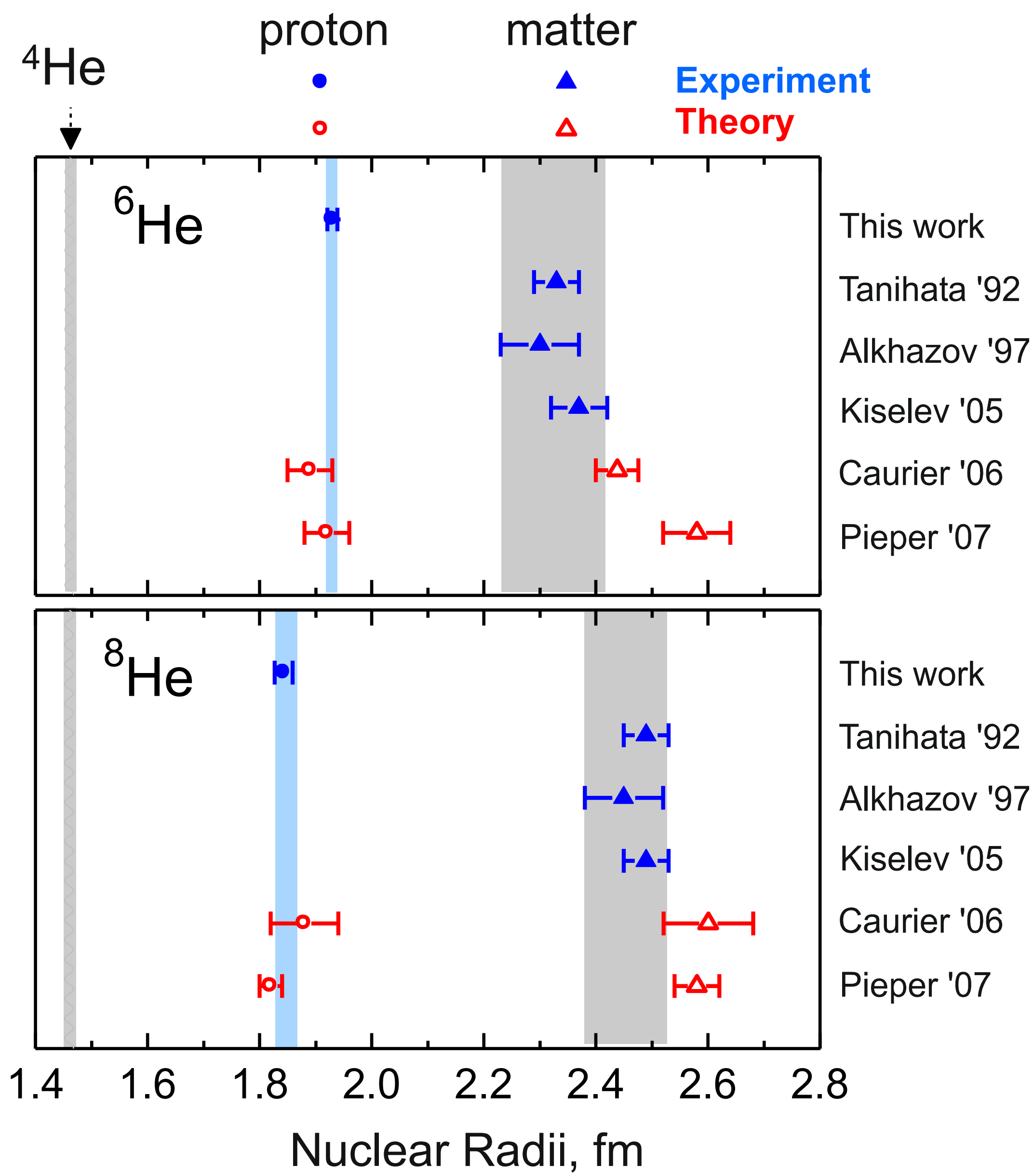

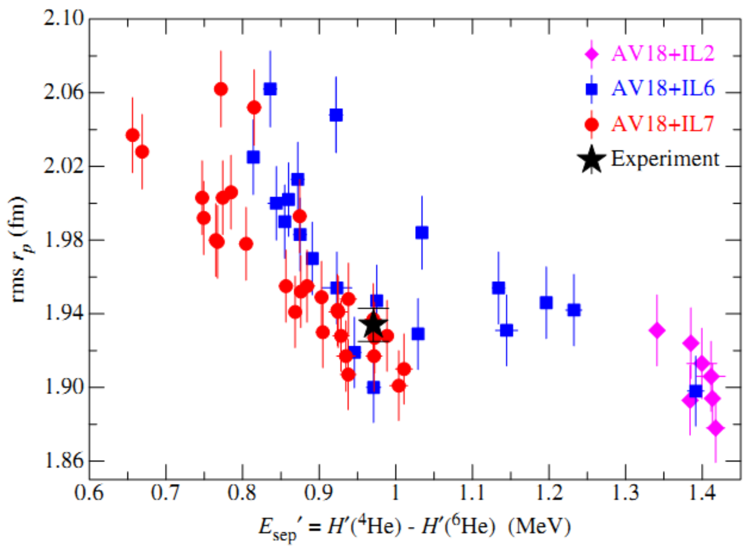

FIG. 9 (color online). ^6He point-proton radius vs two-neutron separation energy obtained from a number of GFMC calculations with different initial conditions and three-body potentials.

Steve Pieper wrote in RMP (2013)

GFMC calculations using AV18 with the Illinois V_{ijk} are successful in reproducing the energies of nuclear states for $A \leq 12$ (Pieper, Wiringa, and Carlson, 2004; Pieper, 2005, 2008b). The He isotope energies and corresponding two-neutron separation energies E_{2n} obtained for AV18 + IL7 are given in Table V. Quantities other than energy may converge at a much slower pace. This is particularly true for the radii of weakly bound states. For ^8He, and especially for ^6He, there are long-term fluctuations in the radii as GFMC calculations propagate in imaginary time. These fluctuations are associated with the small two-neutron separation energies; according to the calculations, $E_{sep} = 0.97$ MeV for ^6He and 1.86 MeV for ^8He. Figure 9 displays the results of multiple GFMC calculations with different initial conditions. Even though GFMC can compute the binding energies precisely, its relative errors in E_{sep} are significant since, for ^6He, E_{sep} is only 3% of the binding energy. For example, changes in the starting wave function Ψ_T and other aspects of the GFMC calculations can result in changes of 0.2 MeV in E_{sep}, or a few percent change in the radius. For these weakly bound nuclei, more precise values of radii can be obtained by selecting those calculations that simultaneously yield the experimentally known E_{sep} value, marked with a star in Fig. 9, with its associated range interpreted as an uncertainty of the computed radii. The same procedure is used to get the matter radii r_m (Table VI). The computed point-proton radii

Proton- & Matter-Radii of ^{6}He & ^{8}He

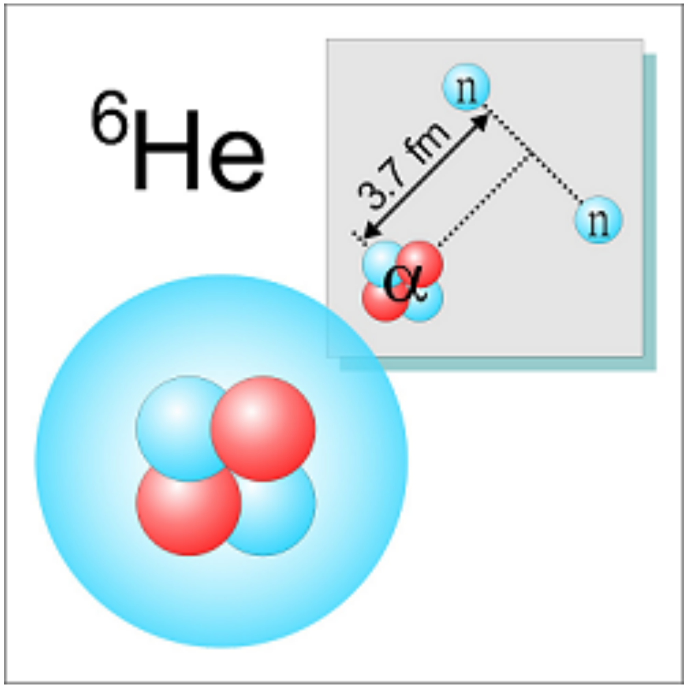

Lu *et al.*, RMP (2013)

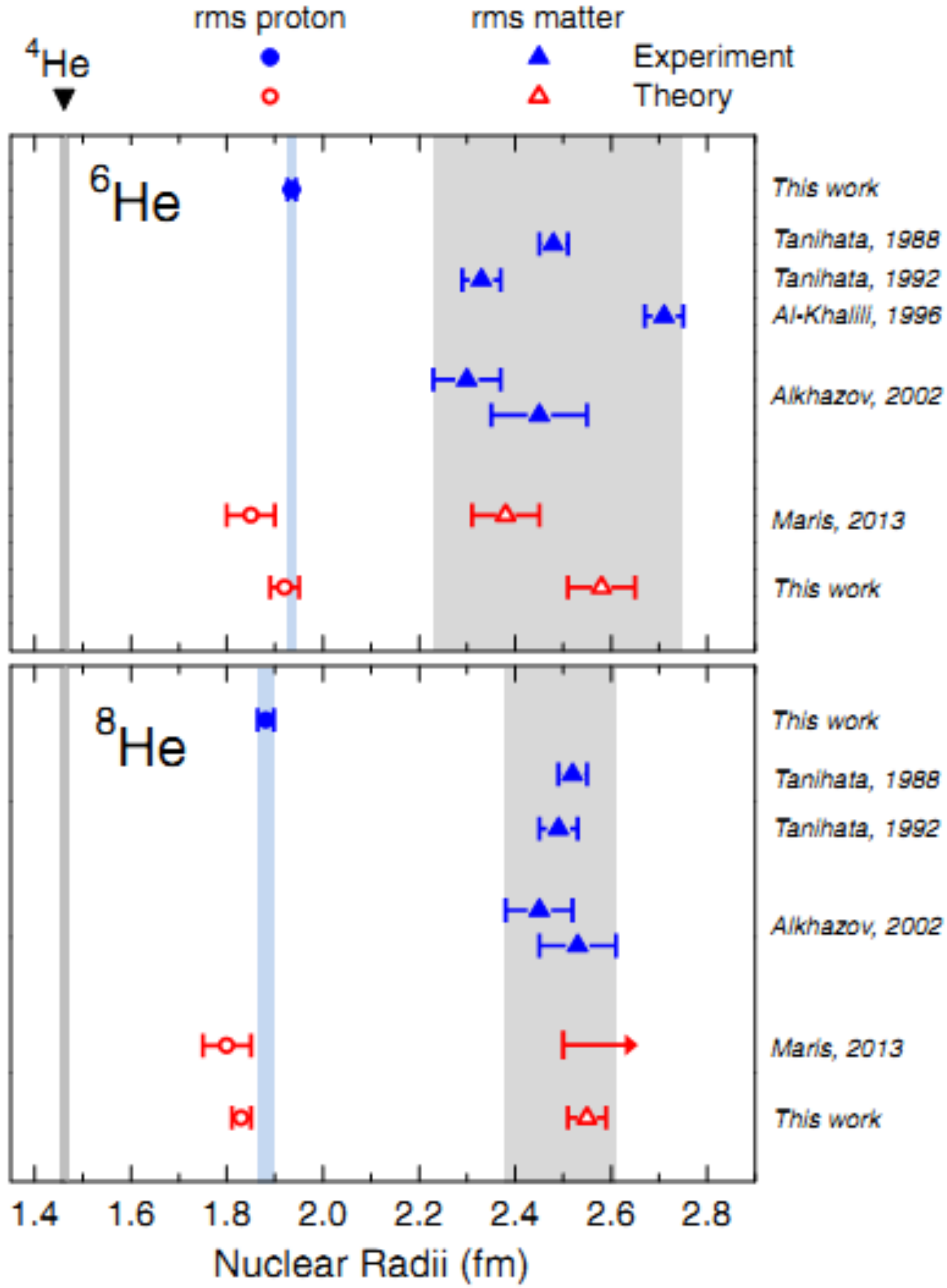

Atom Trap Trace Analysis –
Method and Applications in the Earth Sciences

Zheng-Tian Lu

Department of Modern Physics
University of Science and Technology of China (USTC)

Hefei National Laboratory for Physical Sciences at the Microscale

CAS Center for Excellence in Quantum Information
and Quantum Physics

ICEQT September 2019

創寰宇學府
育天下英才
嚴濟慈題
一九八八年五月

中国科学技术大学
University of Science and Technology of China

Atom Trap Trace Analysis (ATTA) - Krypton

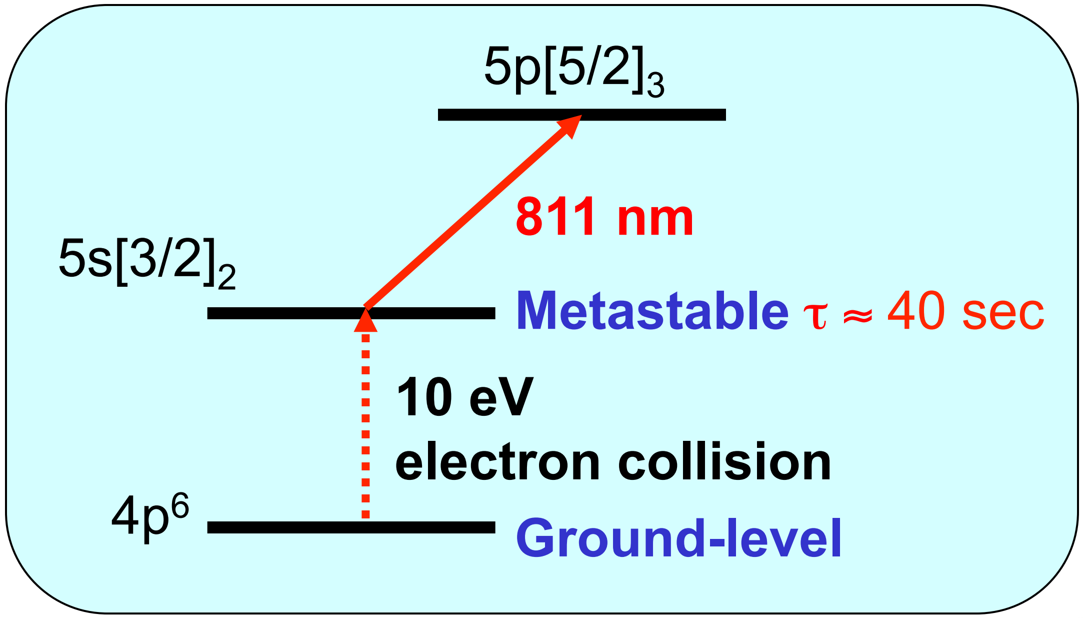

CCD image profile of a single ^{81}Kr atom

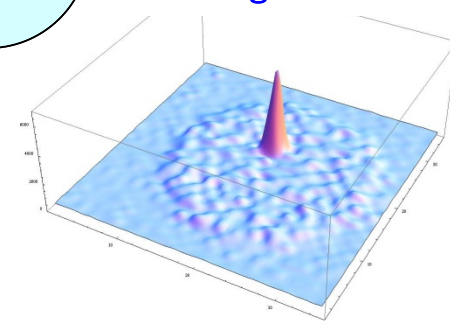

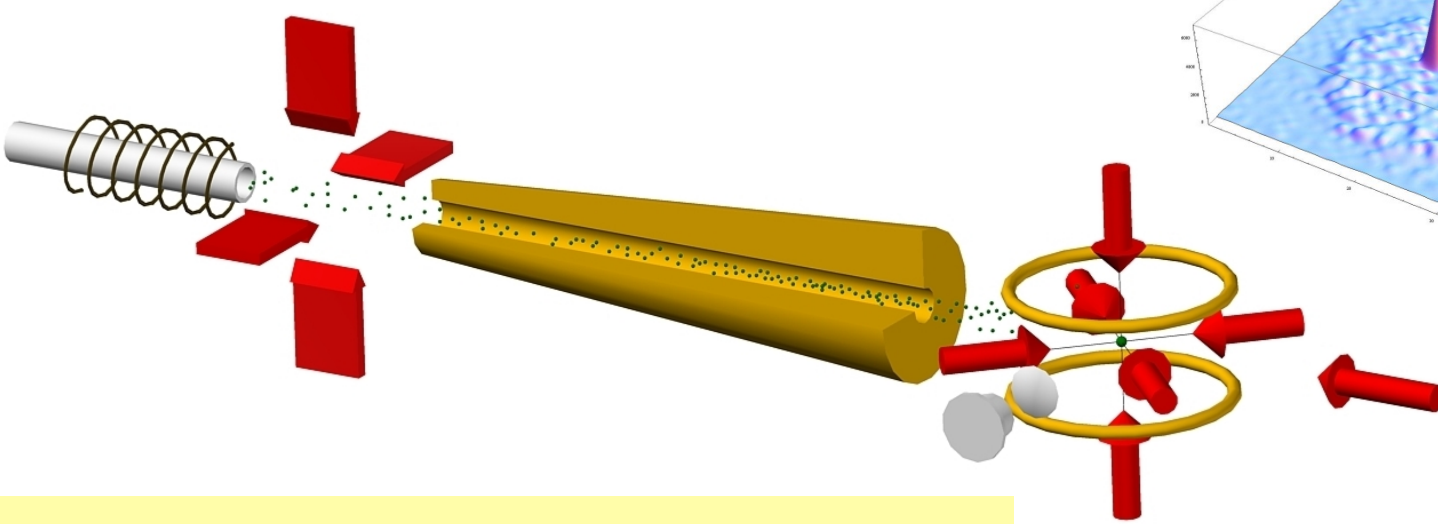

Ultrasensitive isotope trace analyses with a magneto-optical trap

Chen *et al.*, Science 286, 1139 (1999)

Collaboration of Earth Science and Physics

Sampling & sample prep

- Bern, Switzerland
- U. Chicago, U.S.
- IAEA, Vienna
- USTC, China
- Heidelberg, Germany
- U. Delaware, U.S.
- CSIRO, Australia
- Hamburg, Germany
- ……

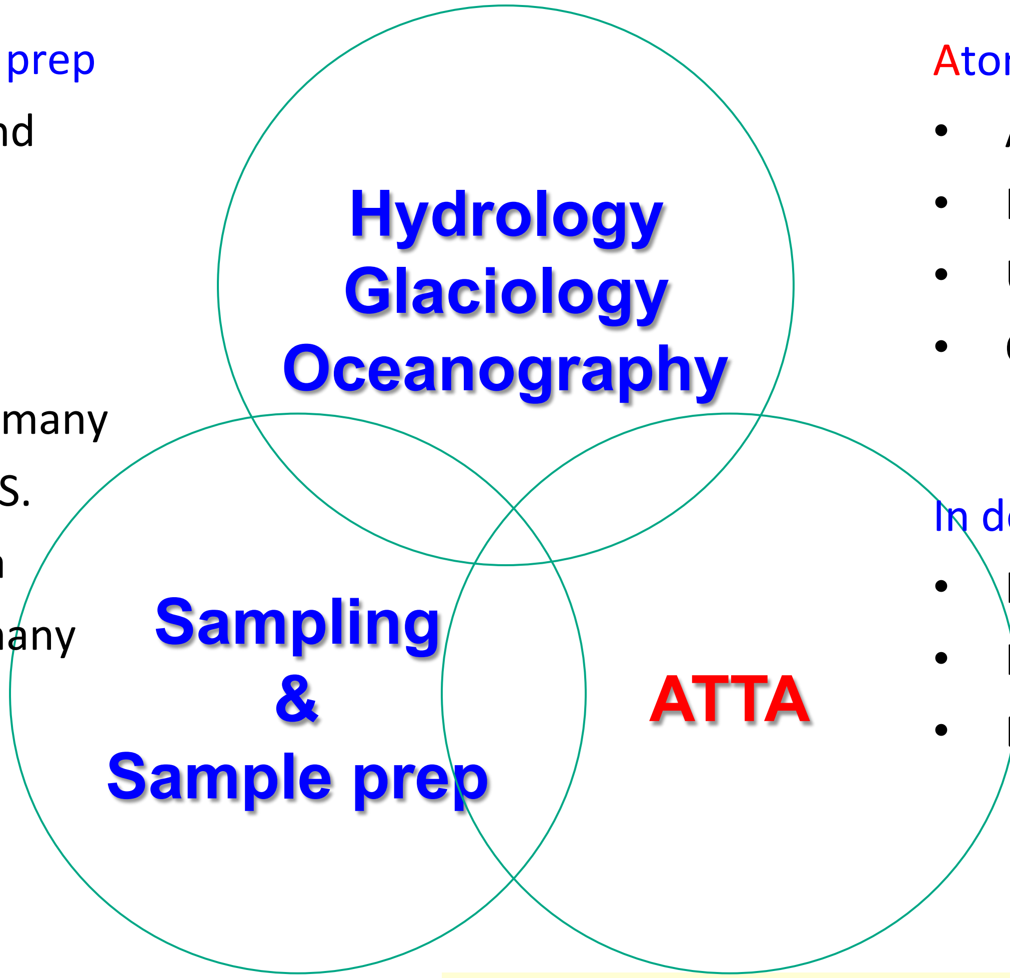

Atom Trap Trace Analysis

- Argonne, U.S.
- Heidelberg, Germany
- USTC, China
- CSIRO, Australia

In development

- IAEA, UN
- Hamburg, Germany
- Bern, Switzerland

Google "ATTA Primer"

Radioactive gas isotopes for tracing and dating

- **Gas:** Even distribution around the world
- **Inert:** Simple production, transport and deposition process

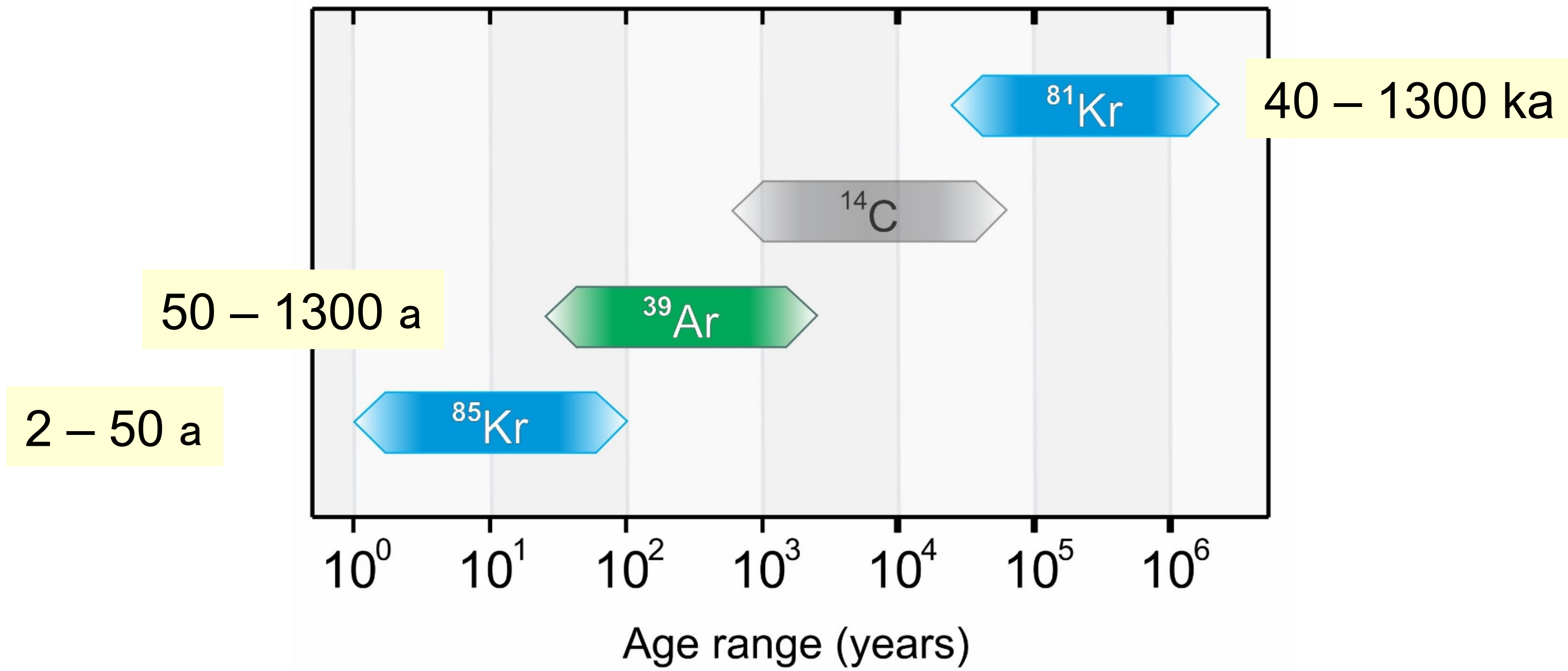

^{85}Kr, ^{39}Ar, ^{81}Kr: Ideal isotopes for dating / tracing

Water/Ice sample size needed over the years

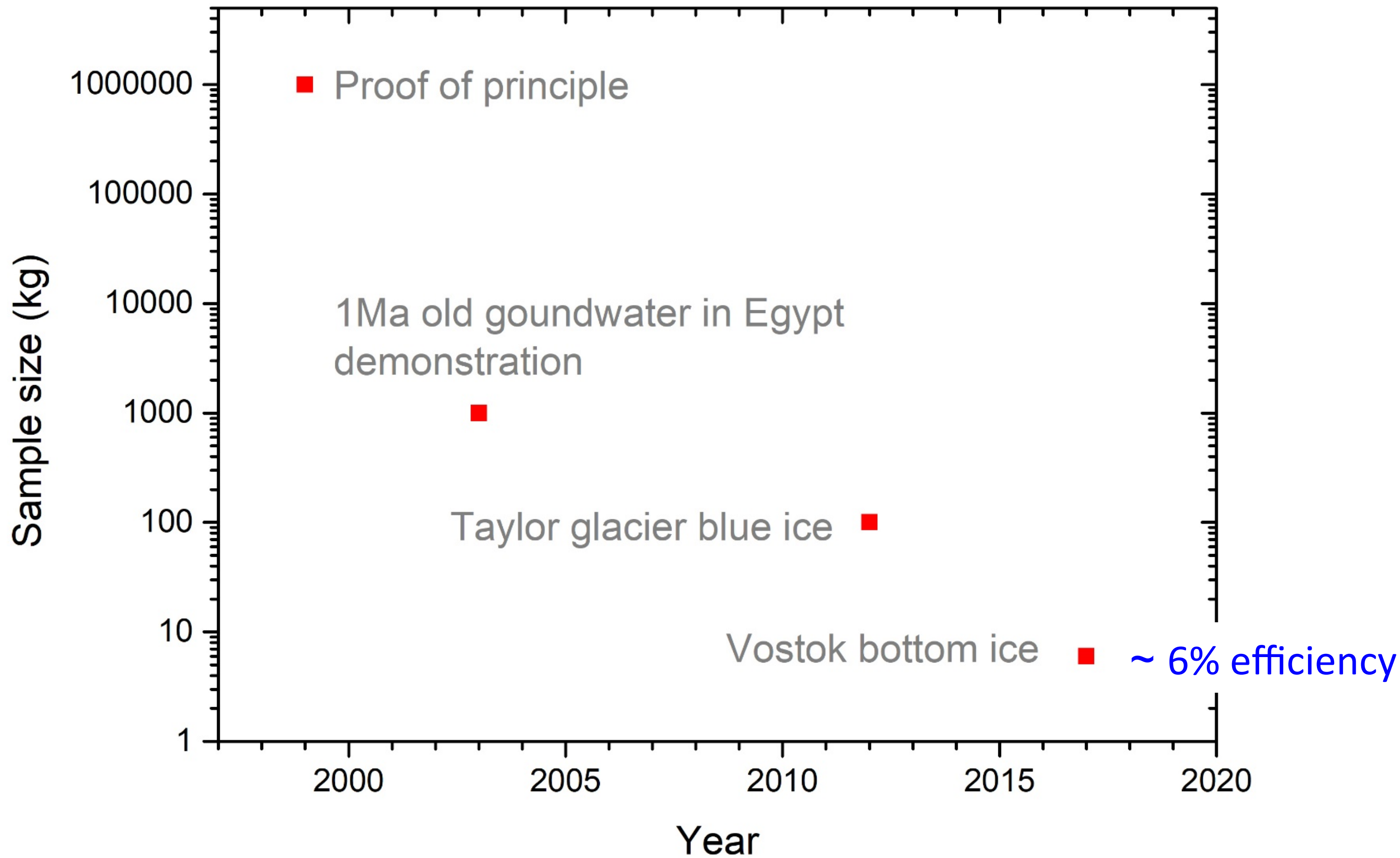

ATTA Instrument for Kr-81 at USTC

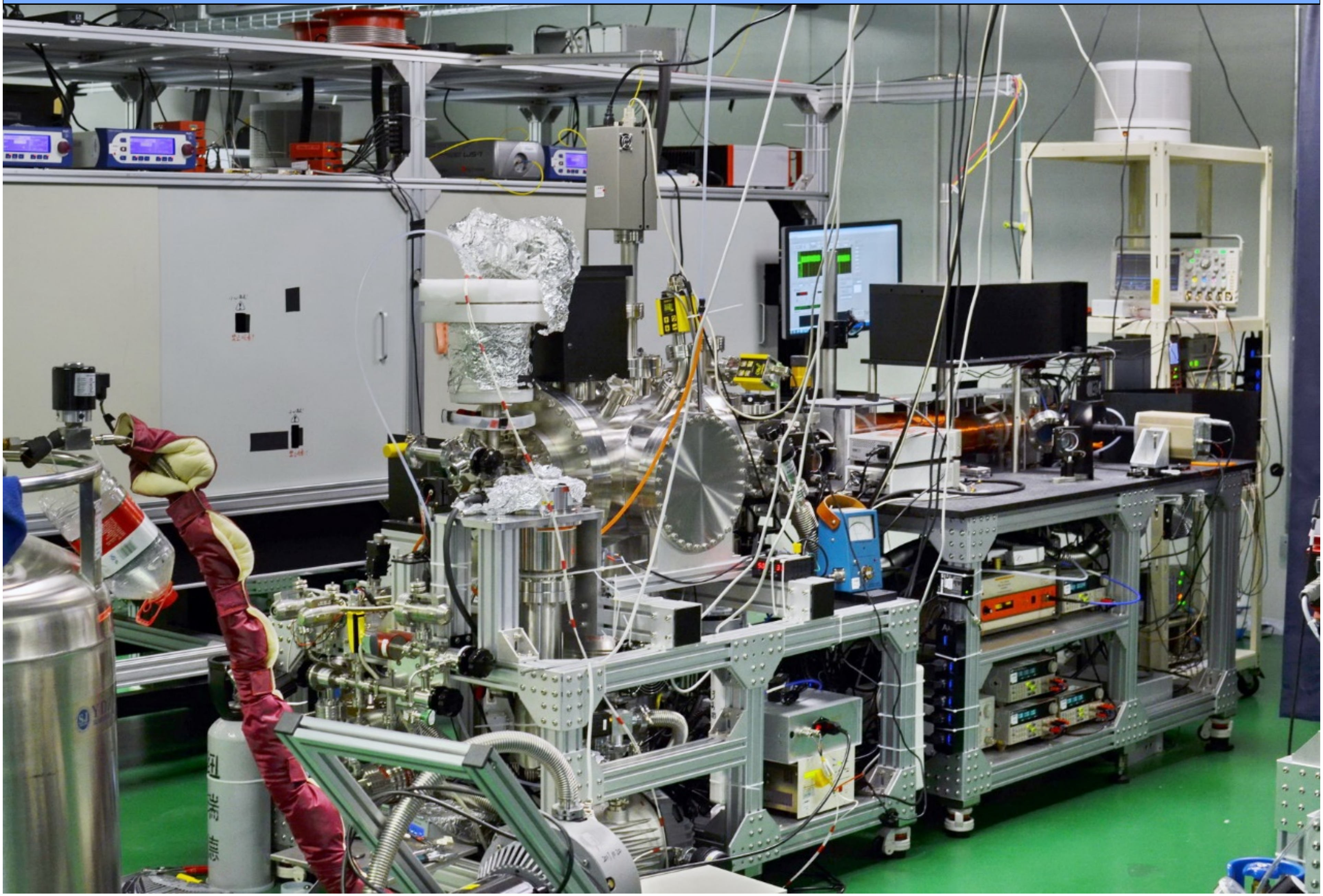

USTC ATTA Lab (2019)

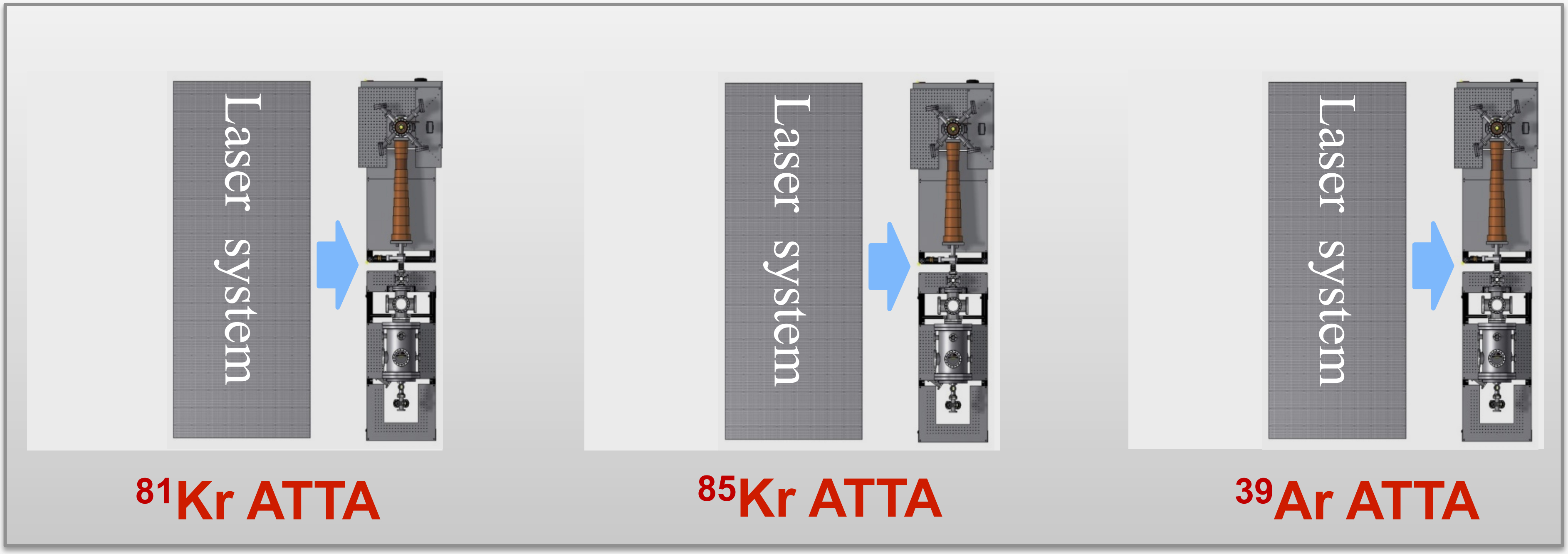

- 1x Kr-81 beamlines, 200 samples/year
- 1x Kr-85 beamlines, 500 samples/year
- 1x Ar-39 beamlines, 200 samples/year

USTC ATTA Lab (2021)

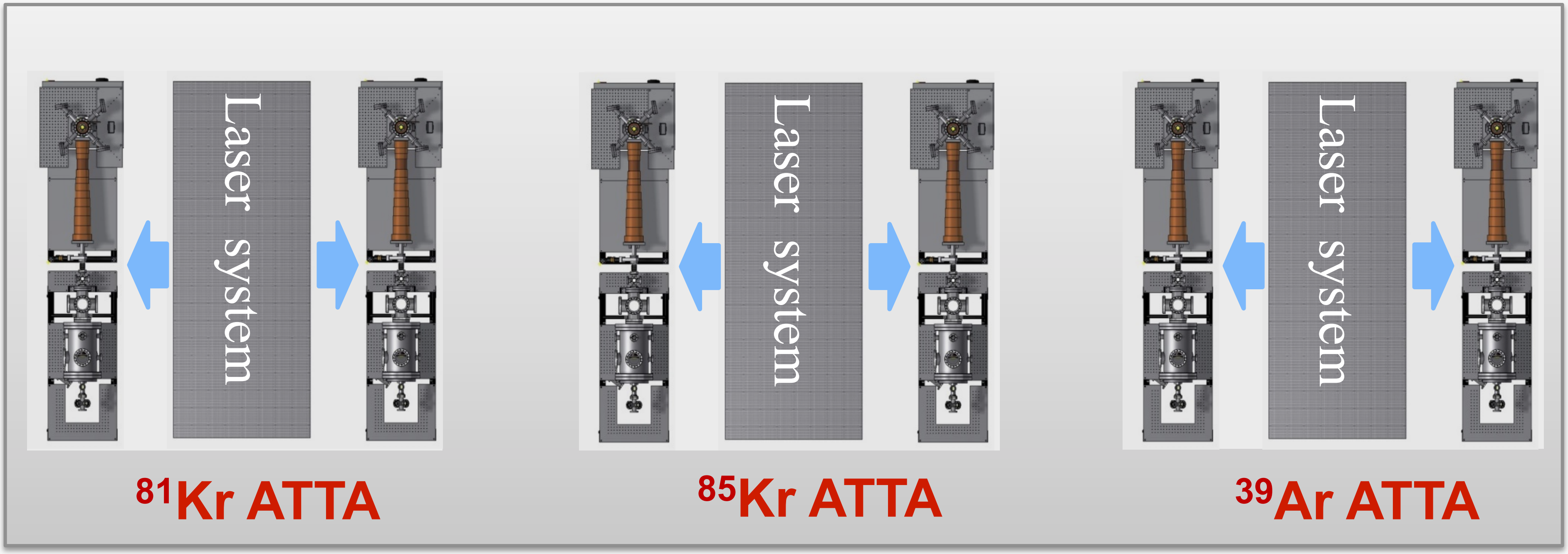

- 2x Kr-81 beamlines, 400 samples/year
- 2x Kr-85 beamlines, 1000 samples/year
- 2x Ar-39 beamlines, 400 samples/year

IAEA Water Resources Programme

Groundwater Resources of the World

- Large Aquifer Systems -

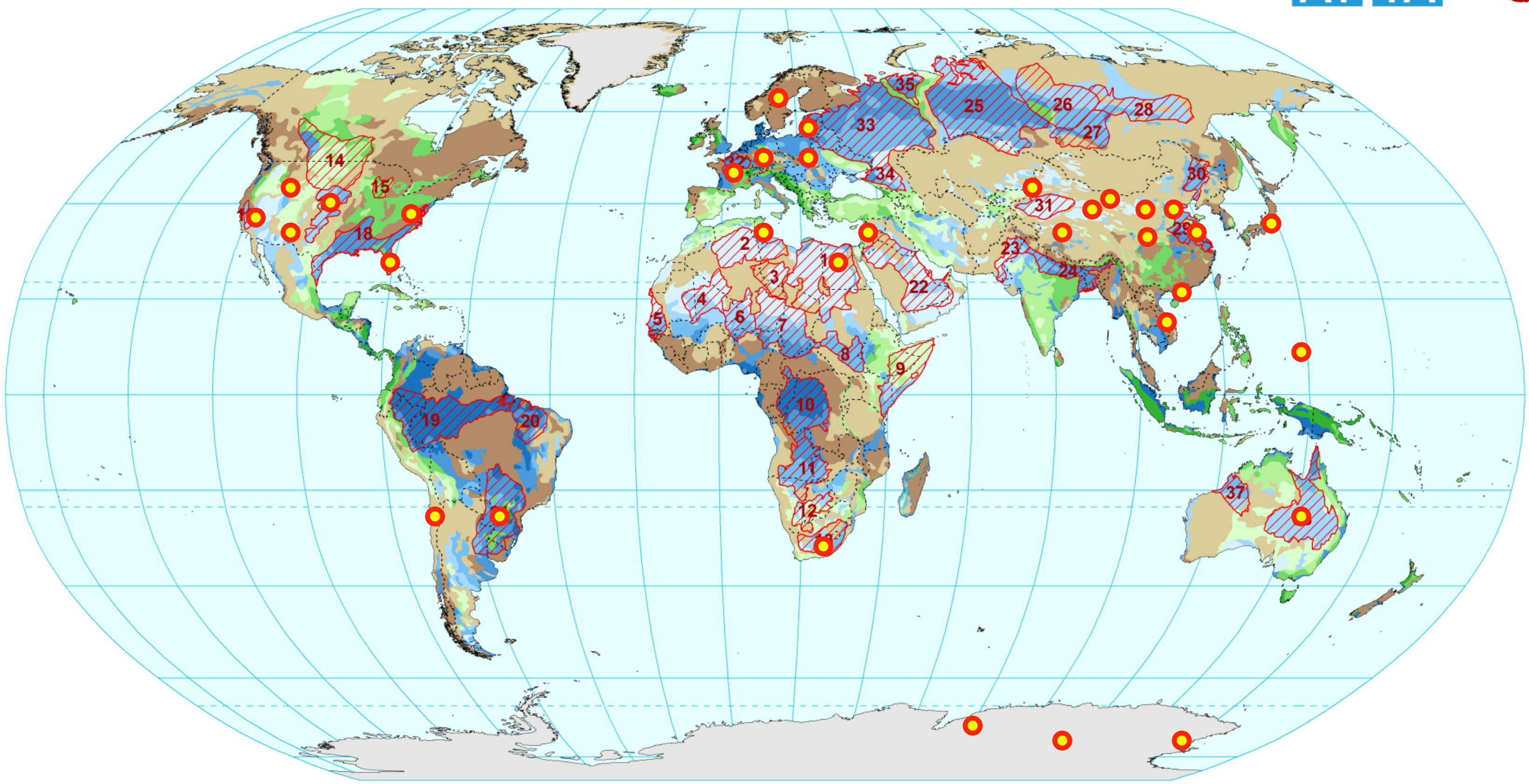

Large Aquifer Systems

1. Nubian Aquifer System (NAS)
2. Northwest Sahara Aquifer System (NWSAS)
3. Murzuk-Djado Basin
4. Taoudeni-Tanezrouft Basin
5. Senegalo-Mauritanian Basin
6. Iullemeden-Irhazer Aquifer System
7. Chad Basin
8. Sudd Basin (Umm Ruwaba Aquifer)
9. Ogaden-Juba Basin
10. Congo Intracratonic Basin
11. Northern Kalahari Basin
12. Southeast Kalahari Basin
13. Karoo Basin
14. Northern Great Plains / Interior Plains Aquifer
15. Cambro-Ordovician Aquifer System
16. California Central Valley Aquifer System
17. High Plains-Ogallala Aquifer
18. Gulf Coastal Plains Aquifer System
19. Amazonas Basin
20. Maranhao Basin
21. Guarani Aquifer System
22. Arabian Aquifer System
23. Indus Basin
24. Ganges-Brahmaputra Basin
25. West Siberian Artesian Basin
26. Tunguss Basin
27. Angara-Lena Artesian Basin
28. Yakut Basin
29. North China Plain Aquifer System
30. Songliao Basin
31. Tarim Basin
32. Parisian Basin
33. East European Aquifer System
34. North Caucasus Basin
35. Pechora Basin
36. Great Artesian Basin
37. Canning Basin

Groundwater resources

groundwater recharge (mm/a): very high – 300 – high – 100 – medium – 20 – low – 2 – very low – 0

- in major groundwater basins
- in areas with complex hydrogeological structure
- in areas with local and shallow aquifers

Groundwater

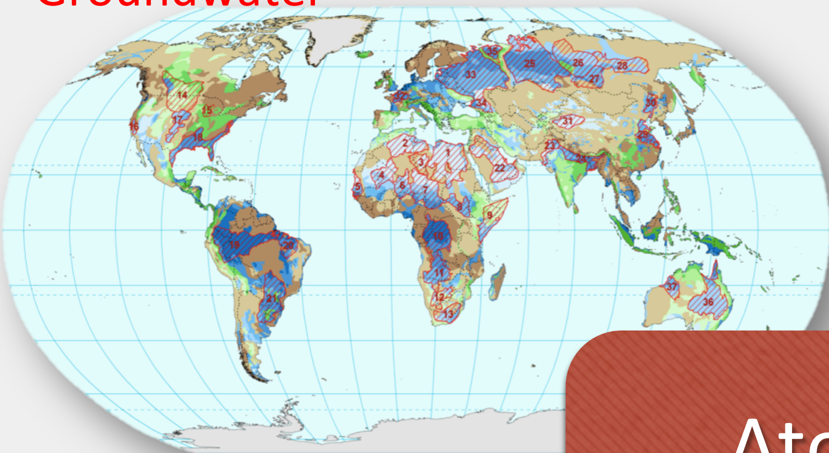

Ocean

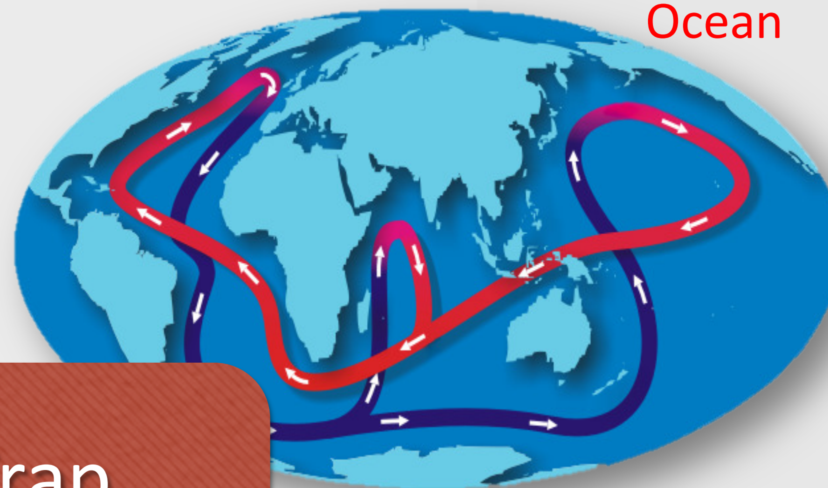

Atom Trap Trace Analysis

Glacier

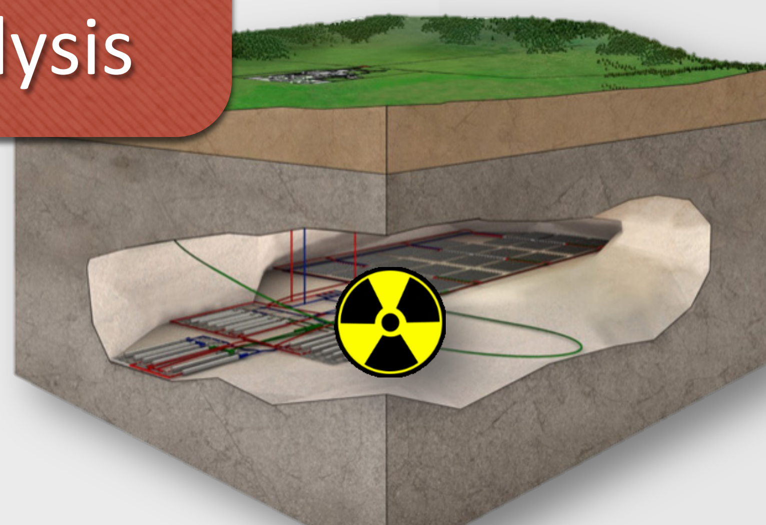

Nuclear safety


China National
Nuclear Corp
北山
^{81}Kr characterize old (isolated) groundwater environment
for sites of nuclear waste repository
• Waste Isolation Pilot Plant (WIPP), New Mexico, USA
• China National Nuclear Corp., Beishan, China
• Central Res. Inst. of Electric Power Industry (CRIEPI), Japan
Beishan, China

Vostok Ice Core

- Depth : Below 3500m
- 3 Consecutive samples
- Weight : ~ 6 kg!

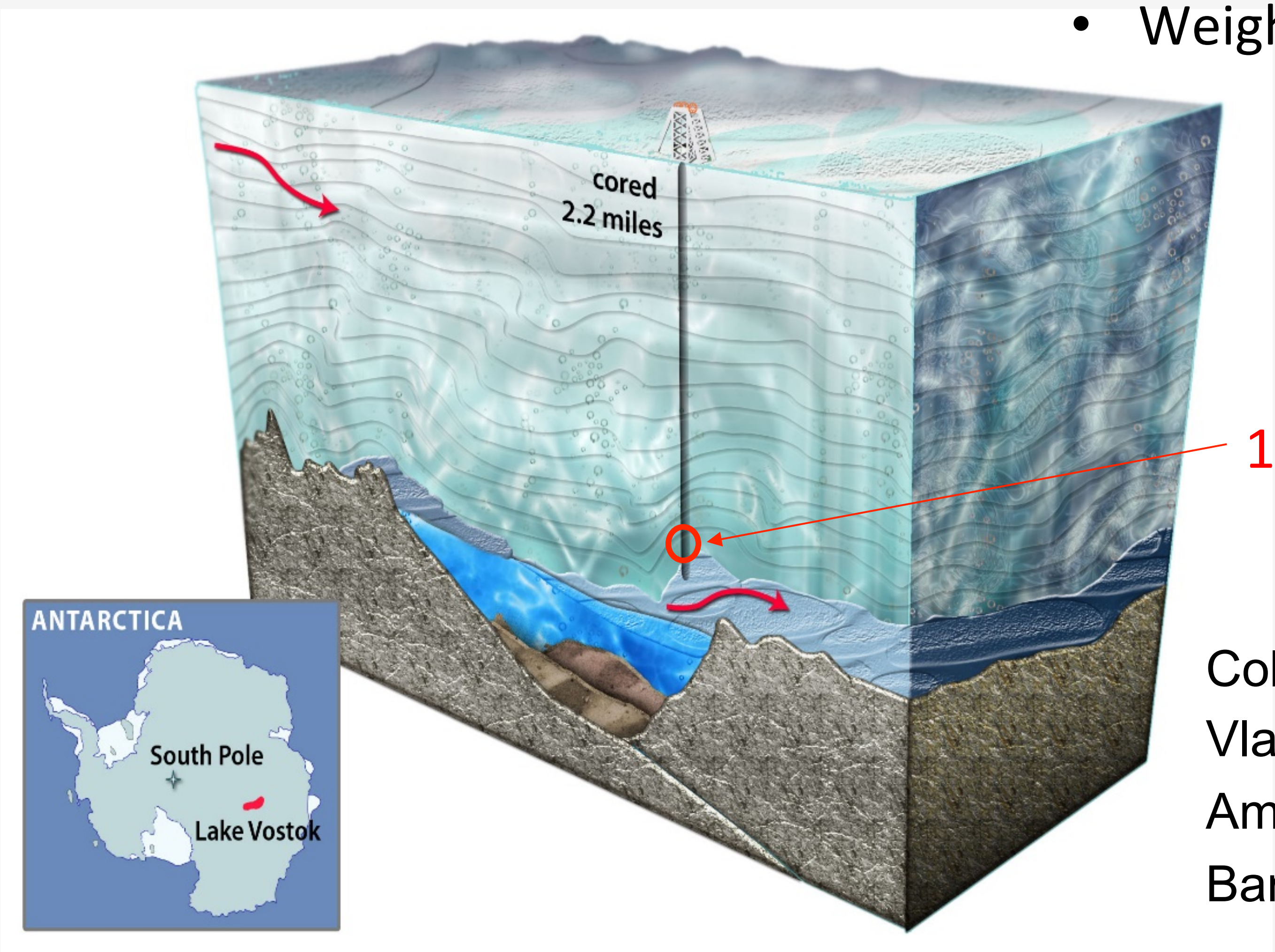

1 million years old

Collaborators:
Vladimir Lipenkov, AARI
Amaelle Landais, LSCE
Barbara Stenni, Venice

With Laboratory for Sciences of Climate and Environment （LSCE）
Arctic and Antarctic Research Institute（AARI）

Guliya Ice Cap

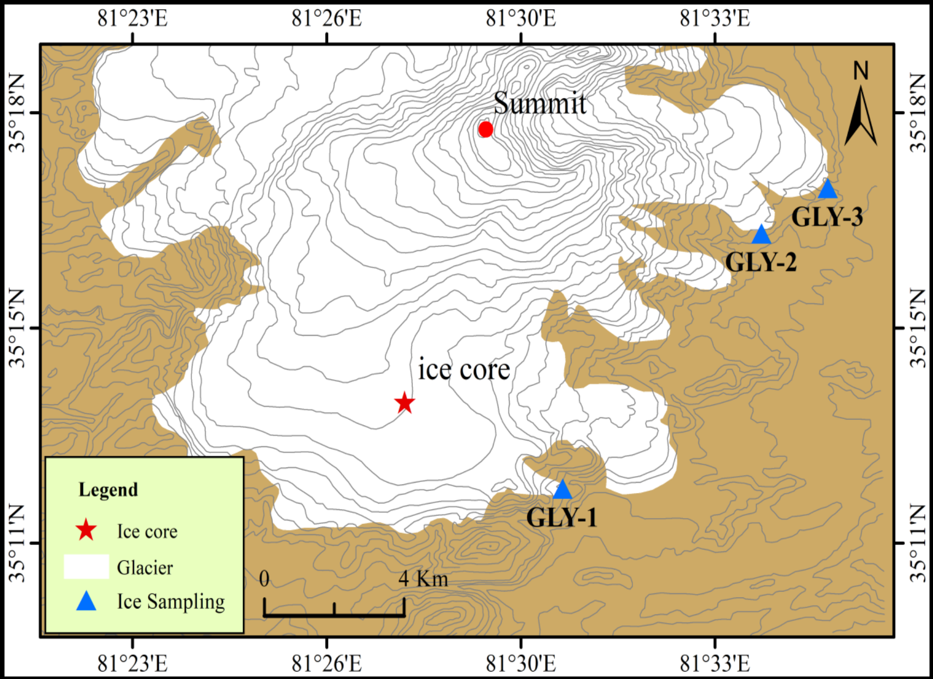

^{81}Kr ages of 8 samples
Ages < 15 - 74 ka

Li-De Tian *et al.*,
Geophys. Res. Lett. (2019)

First ^{39}Ar-dating of small ocean samples

Heidelberg University (Markus Oberthaler and Werner Aeschbach)
GEOMAR Kiel (Toste Tanhua)

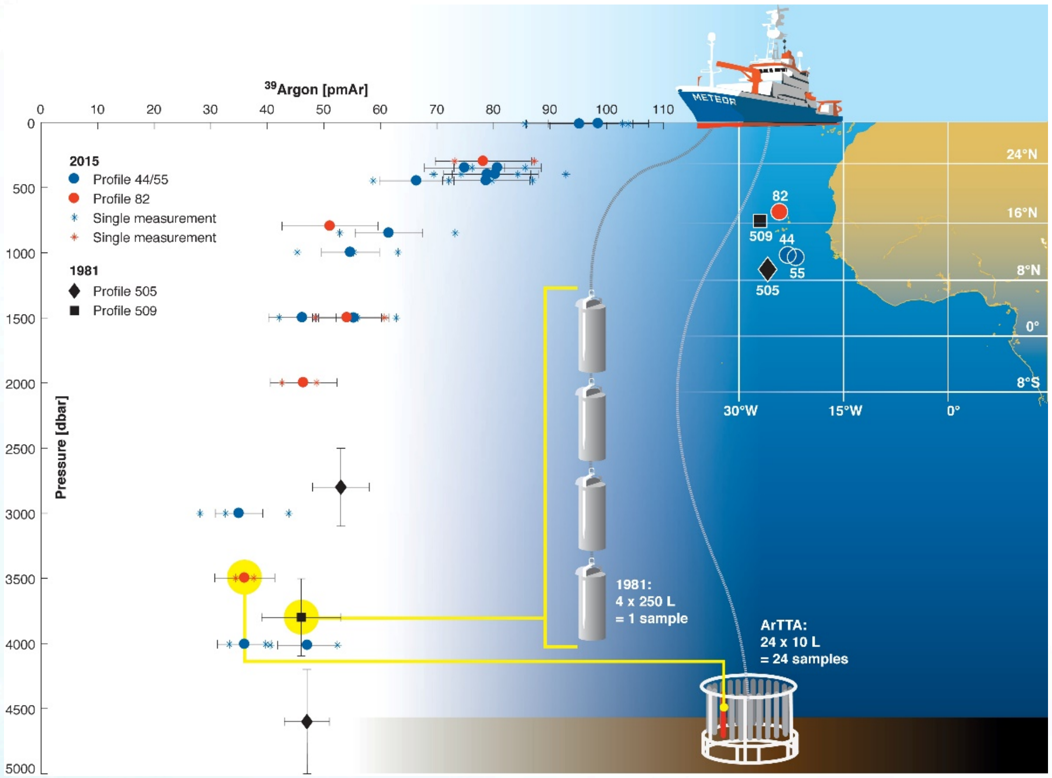

Ebser, S. et al., *Nat. Commun.* **9**, 5046 (2018)

Sampling:

- Three depth profiles from the North Atlantic
  (Eastern tropical North Atlantic Oxygen Minimum Zone)
- 5 liters of water per data point
- Sampling with standard Niskin bottles

Main results:

- ^{39}Ar & CFC constrain transit time distributions
- Mean ages of up to 800 years
- Reveal ocean ventilation patterns
- Advection in intermediate depths much more important than previously assumed

PPT by Sven Ebser

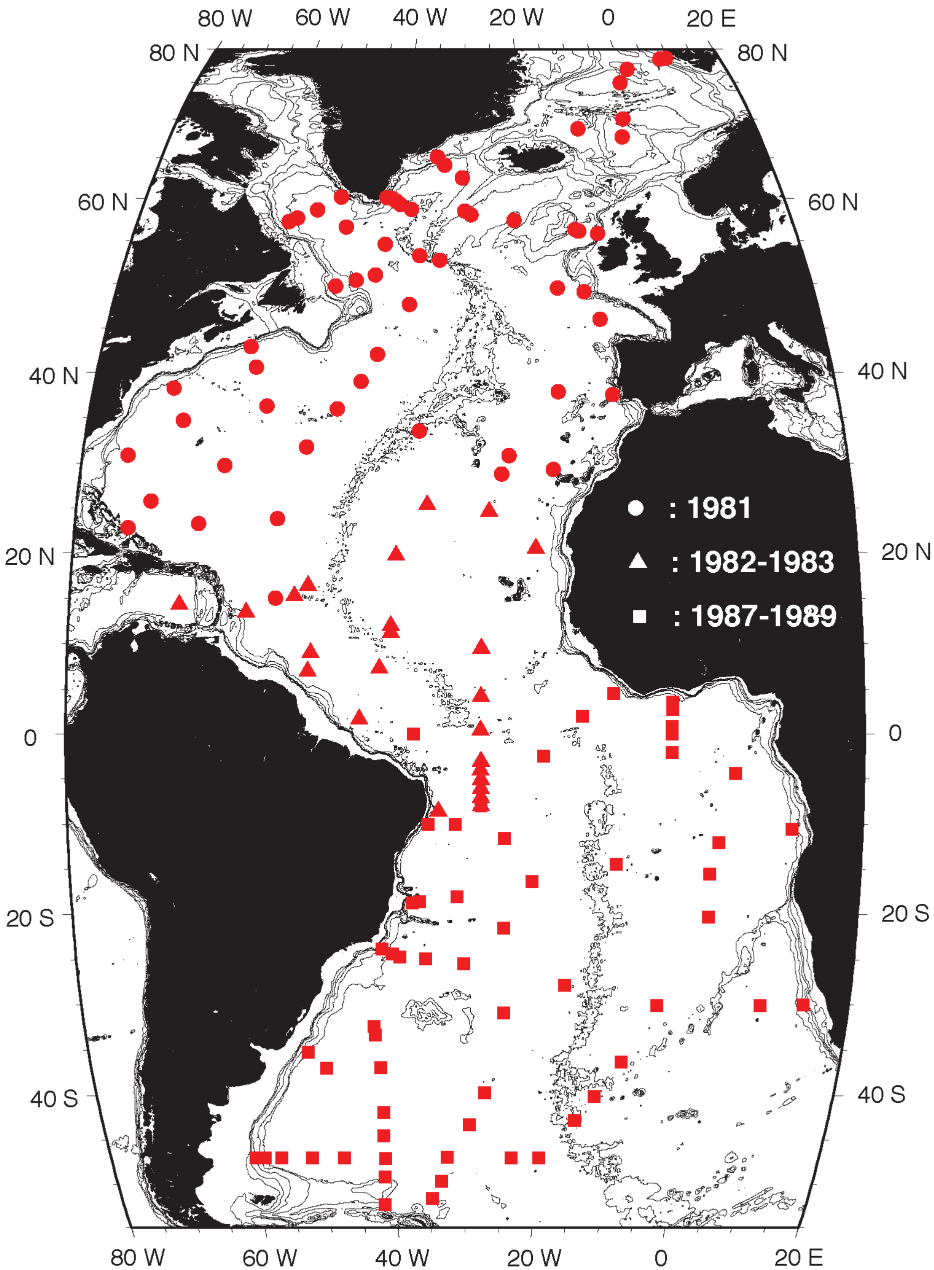

Z.-T. Lu *et al.*, Earth-Sci. Rev. (2014)

Lamont-Doherty Earth Observatory
Columbia University
William Smethie Jr., Martin Stute *et al*.

- 900 Atlantic samples collected in the 80's
- ^{39}Ar dating by USTC and Heidelberg

"a more dense survey of ^{39}Ar with higher accuracy measurements would prove of great value in constraining ocean general circulation models."
--- Broecker and Peng (2000)

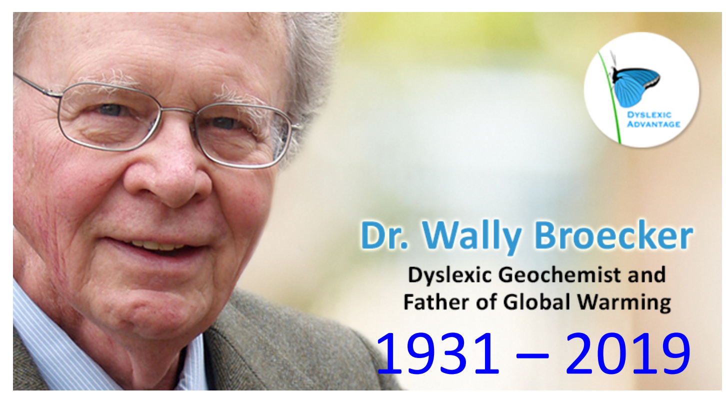

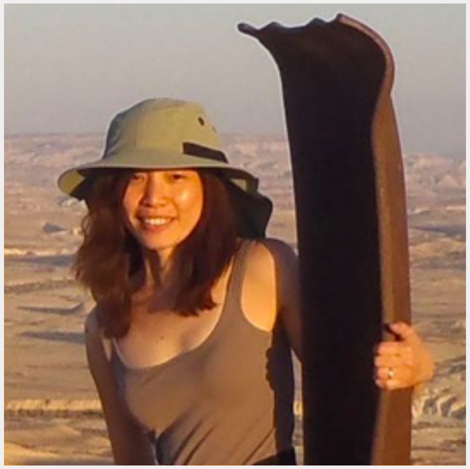

Radiokrypton unveils dual moisture sources of a deep desert aquifer

Yokochi *et al*., PNAS 116, 16222 (2019)

Reika Yokochi
U Chicago

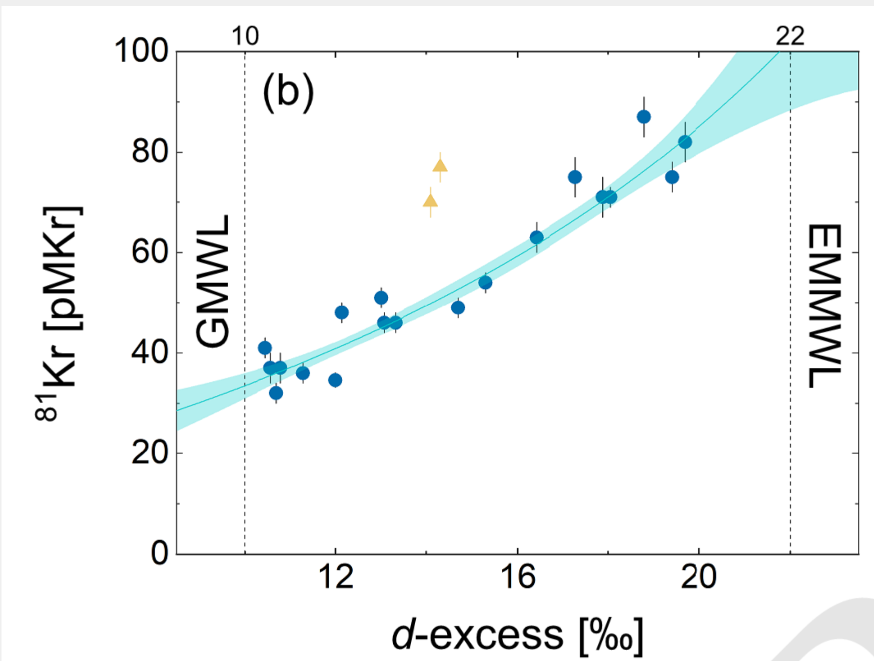

- Investigated the paleo-hydroclimate properties of the Nubian Sandstone Aquifer in the Negev Desert, Israel.
- Resolved subsurface mixing and identified two distinct moisture sources of recharge.
- Reveals that tectonically active terrain can store groundwater.

Atlantic ocean
361±30 ka

Mediterranean
< 38 ka


August 13, 2019 | vol. 116 | no. 33 | pp. 16153–16656
PNAS
Proceedings of the National Academy of Sciences of the United States of America
www.pnas.org
Groundwater source tracing using radiokrypton
High-pressure methane hydrate phase
Injected fluid diffusion and induced seismicity
Social genetic effects on adolescent smoking
Yeast antiviral pathway and apoptosis

^{81}Kr in the Atmosphere

- production rate and abundance

(A) Geomagnetic field

(B) Production rate

(C) ^{81}Kr age correction

< 4%

-- C. Buizert *et.al.,* Proc. Natl. Acad Sci. **111**, 6876 (2014)

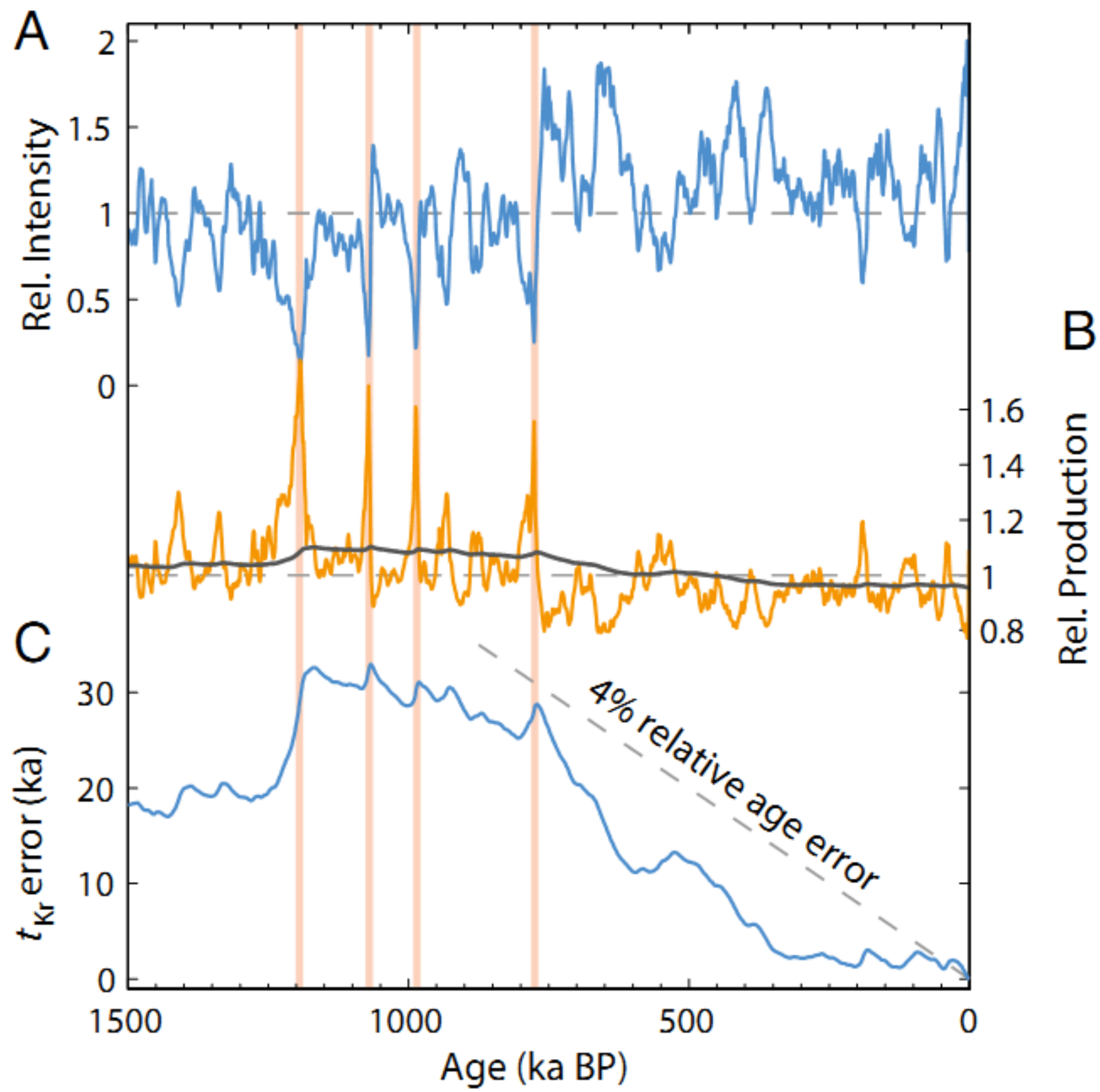

Fig. 3. Stability of atmospheric ^{81}Kr. (*A*) Relative paleointensity of the geomagnetic field (56). Magnetic reversals are indicated by vertical lines. (*B*) Relative spallogenic production rate (orange) with relative ^{81}Kr abundance (black). The ^{81}Kr abundance is calculated through a convolution of the production rate with the atmospheric ^{81}Kr residence [1/330 × exp(−*t*/330), with time *t* in ka]. (*C*) Estimated error in ^{81}Kr radiometric age when assuming stable atmospheric ^{81}Kr/Kr; positive values indicate an underestimated t_{Kr}.